Single-Λ_c^+ hypernuclei within a quark mean-field model

Linzhuo Wu, Jinniu Hu,* and Hong Shen
School of Physics, Nankai University, Tianjin 300071, China

(Received 20 September 2019; revised manuscript received 15 December 2019; accepted 23 January 2020; published 10 February 2020)

The quark mean-field (QMF) model is applied to study the single-Λ_c^+ hypernuclei. The charm baryon Λ_c^+ is constructed by three constituent quarks, u, d, and c, confined by central harmonic oscillator potentials. The confinement potential strength of charm quark is determined by fitting the experimental masses of charm baryons, Λ_c^+, Σ_c^+, and Ξ_{cc}^{++}. The effects of pions and gluons are also considered to describe the baryons at the quark level. The baryons in Λ_c^+ hypernuclei interact with each other through exchanging the σ, ω, and ρ mesons between the quarks confined in different baryons. The Λ_c^+N potential in the QMF model is strongly dependent on the coupling constant between ω meson and Λ_c^+, $g_{\omega\Lambda_c^+}$. When the conventional quark counting rule is used, i.e., $g_{\omega\Lambda_c^+} = 2/3 g_{\omega N}$, the massive Λ_c^+ hypernucleus can exist, whose single-Λ_c^+ binding energy is smaller with the mass number increasing because of the strong Coulomb repulsion between Λ_c^+ and protons. When $g_{\omega\Lambda_c^+}$ is fixed by the latest lattice Λ_c^+N potential, the Λ_c^+ hypernuclei only can exist up to $A \approx 50$.

DOI: 10.1103/PhysRevC.101.024303

I. INTRODUCTION

The strangeness degree of freedom was studied from the early 1950s to explain the strange particles and hypernucleus observed in the cosmic rays [1]. After the quark models were proposed by Gell-Mann and Zweig in 1960s, it was regarded that the strangeness in nuclear physics was generated by the strange (s) quark. With the developments of accelerators and detectors, many Λ hypernuclei with Λ hyperon bound in nuclei were observed in the large nuclear facilities in the past half century [2–4] from ${}^{3}_{\Lambda}$H to ${}^{208}_{\Lambda}$Pb. The Σ hypernuclei were not detected except the ${}^{4}_{\Sigma}$He quasibound state [5,6]. It was generally considered that the ΣN interaction is repulsive. Furthermore, there were also some experimental evidences to indicate the existence of Ξ hypernuclei [7–11] and few $\Lambda\Lambda$ light hypernuclei [12–15].

The hyperons do not have to obey the Pauli exclusion principle in the normal nuclear system, which can be easily bound in a nucleus. Therefore, the hypernucleus is a good probe to investigate the baryon-baryon interaction [16–19]. Many new-generation facilities, such as, FAIR, JLab, J-PARC, MAMI, and HIAF are planning to explore more unknown Λ hypernuclei in the nuclear landscape [3]. In the aspect of theoretical researches, various nuclear models were applied to study the hypernuclei, such as the *ab initio* methods for light hypernuclei [20,21], G-matrix calculation [22], shell model [23], Skyrme-Hartree-Fock model [24–27], relativistic mean-field model [28–34], quark meson-coupling model [35–37], quark mean-field model [38–40], and so on for heavy hypernuclei. These models can describe the ground-state properties of Λ hypernuclei very well with various effective ΛN interactions.

In addition to the up, down, and strange quarks, there are also charm, bottom, and top quarks in the universe, which can combine with the up and down quarks to constitute exotic baryons. The Λ_c^+ was the first charmed baryon confirmed in experiment, whose components are very similar to the Λ hyperon [41]. Only the strange quark is replaced by charm quark in Λ_c^+. A natural question is whether Λ_c^+ and normal nuclei can bind together to form a charmed hypernuclei. Actually, 40 years ago, Dover and Kahana already discussed the possibility of charmed hypernuclei with a Λ_c^+N potential generated by SU(4) symmetry, where the bound states of a charmed baryon and normal nuclei were predicted [42]. Then, the light charmed hypernuclei were investigated by cluster model and few-body methods [43–46]. The heavy nuclei are better described by the density functional theory. Accordingly, the massive charmed hypernuclei were calculated by the quark meson-coupling (QMC) model [47–50] and the relativistic mean-field (RMF) model [51,52]. The binding energies, density distribution, impurity effect, and medium effect of charmed hypernuclei were widely discussed in these works. Meanwhile, the investigations of Λ_c^+ hypernuclei in the aspect of experiment were explored in the 1970s and 1980s in Dubna, which only reported three possible candidate events because of the difficult production mechanism of charmed hypernuclei [53–55]. In the future, FAIR and JPARC are hopefully expected to produce sufficient charmed particles to generate more charmed hypernuclei [56–58].

The essential element to determine the properties of charmed hypernuclei is the strength of Λ_c^+N potential. In the early time, it was obtained by extending the one-boson-exchange potential (OBEP) for nucleon-nucleon and nucleon-hyperon systems with SU(4) symmetry [42]. Recently, Liu and Oka considered a more reasonable Lagrangian of OBEP to include the chiral symmetry, heavy quark symmetry, and hidden local symmetry [59,60]. In QMC and RMF models, the coupling constants between charm baryons and mesons were usually generated by the naive quark counting rules.

*hujinniu@nankai.edu.cn

The more reliable and cheerful progress about $\Lambda_c^+ N$ potential was from the lattice QCD simulation. The HAL QCD Collaboration calculated the central and tensor components of the $\Lambda_c^+ N$ potential at $^1S_0$ and $^3S_1$-$^3D_1$ channels within $(2+1)$-flavor lattice QCD at quark masses corresponding to pion masses, $m_\pi \simeq 410,\ 570,\ 700$ MeV, respectively. It was found that the $\Lambda_c^+ N$ potentials with such quark masses were attractive at $^1S_0$ and $^3S_1$ channels [61–65]. Later, Haidenbauer and Krein extrapolated the $\Lambda_c^+ N$ potential at physical pion mass with chiral effective field theory from the HAL QCD results at large quark masses. They also claimed that the $\Lambda_c^+ N$ potential at $m_\pi = 138$ MeV could make the four-body and five-body charmed hypernuclei bind [66]. Garcilazo *et al.* also compared the $\Lambda_c N$ potentials based on different theoretical models including the HAL QCD simulations. They found that these potentials qualitatively agree with each other [67]. With these achievements, Miyamoto *et al.* derived a single-folding $\Lambda_c^+ N$ potential for Λ_c^+ hypernuclei generated by lattice QCD simulation, where the Λ_c^+ hypernuclei could exist between the mass numbers from $A = 12$ to $A \approx 50$ [65]. Furthermore, Vidaña *et al.* recently also discussed the charmed hypernuclei within a microscopic many-body approach with an SU(4) extension of OBEP from the Jülich hyperon-nucleon potential [68]. It was found that the phase shifts from the B and C models of Ref. [68] agree to those extracted from HAL QCD data at physical pion mass by Haidenbauer and Krein. Furthermore, their results about charmed hypernuclei were also compatible with other theoretical calculations [47–52].

The quark mean-field (QMF) model is a very powerful nuclear many-body method from the quark level. The baryon is regarded to be constructed by three constituent quarks with central confinement potentials. The baryon-baryon interaction in nucleus is realized by exchanging the σ, ω, and ρ mesons between the quarks in different baryons. The QMF model was successfully used to study the properties of normal nuclei, Λ, Ξ hypernuclei and neutron star after including the effects of pions and gluons at the hadron level [69–74].

In this work, we would like to apply the QMF model to study the properties of charmed hypernuclei, especially Λ_c^+ ones. The Λ_c^+ baryon consists of u, d, and c quarks, which are confined by the central harmonic oscillator potentials. The strength of confinement potential for charm quark will be fixed by the experimental masses of charmed baryons. The coupling constants between charm quark and mesons will be determined by two schemes. The first one is decided by the naive quark counting rules. The second one is extracted from the HAL QCD simulations. This article is organized as follows. In Sec. II, the theoretic framework of the QMF model related to charmed hypernuclei is presented. The results and discussions for Λ_c^+ hypernuclei will be shown in Sec. III. The summary and conclusions will be given in Sec. IV.

II. QUARK MEAN-FIELD MODEL FOR CHARMED HYPERNUCLEI

In this section, we will give a brief introduction of the QMF model for charmed hypernuclei. In the QMF model, baryons are composed of three constituent quarks, which are confined by the central confinement potentials. The specific form of such potentials cannot be obtained directly because of the nonperturbative character of QCD theory in the low-energy region. Many phenomenological confinement potentials have been proposed, where the polynomial forms were widely used. In this work, we adopt a harmonic oscillator potential with a mixing scalar-vector structure [70–73],

$$U_q(r) = \tfrac{1}{2}(1+\gamma^0)(a_q r^2 + V_q), \tag{1}$$

where the potential parameters a_q and V_q will be determined by the masses of charmed baryons and q denotes u, d, or c, respectively. In this case, the Dirac equation including the nuclear medium effect for confined quark is written as

$$\begin{aligned}[\gamma^0(\epsilon_q - g_{\omega q}\omega - \tau_3 g_{\rho q}\rho) - \vec{\gamma}\cdot\vec{p} \\ -(m_q - g_{\sigma q}\sigma) - U_q(r)]\psi_q(\vec{r}) = 0.\end{aligned} \tag{2}$$

Here, $\psi_q(\vec{r})$ represents the quark field. σ, ω, and ρ are the classical meson fields, which are exchanged between quarks in different baryons to achieve the baryon-baryon interaction. $g_{\sigma q}$, $g_{\omega q}$, and $g_{\rho q}$ are the coupling strengths of σ, ω, and ρ mesons with quarks, respectively. m_q is the constituent quark mass and τ_3 corresponds to the third component of isospin matrix. This equation can be solved exactly and its ground-state solution of the energy satisfies the eigenvalue condition,

$$(\epsilon_q' - m_q')\sqrt{\frac{\lambda_q}{a_q}} = 3, \tag{3}$$

where

$$\begin{aligned}\epsilon_q' &= \epsilon_q^* - V_q/2, \\ m_q' &= m_q^* + V_q/2, \\ \lambda_q &= \epsilon_q' + m_q' = \epsilon_q^* + m_q^*.\end{aligned} \tag{4}$$

Considering the effect of nuclear medium generated by the meson fields, the effective single-quark energy and effective quark mass are defined by

$$\begin{aligned}\epsilon_q^* &= \epsilon_q - g_{\omega q}\omega - \tau_3 g_{\rho q}\rho, \\ m_q^* &= m_q - g_{\sigma q}\sigma.\end{aligned} \tag{5}$$

The corresponding wave function is

$$\psi_q = \frac{1}{\sqrt{4\pi}}\begin{pmatrix} i g_q(r)/r \\ \vec{\sigma}\cdot\hat{\vec{r}} f_q(r)/r \end{pmatrix}\chi_s, \tag{6}$$

where

$$\begin{aligned}g_q(r) &= \mathcal{N}_q\left(\frac{r}{r_{0q}}\right)e^{-r^2/2r_{0q}^2}, \\ f_q(r) &= -\frac{\mathcal{N}_q}{\lambda_q r_{0q}}\left(\frac{r}{r_{0q}}\right)^2 e^{-r^2/2r_{0q}^2}.\end{aligned} \tag{7}$$

The normalization constant has $\mathcal{N}_q^2 = \frac{8\lambda_q}{\sqrt{\pi}r_{0q}}\frac{1}{3\epsilon_q'+m_q'}$ and $r_{0q} = (a_q\lambda_q)^{-1/4}$. The ground-state energy for quark ϵ_q^* can be obtained by solving Eq. (3). Accordingly, the binding energy of three quarks as the zeroth-order energy of the baryon can be written immediately as

$$E_B^{*0} = \sum_q \epsilon_q^*. \tag{8}$$

Three corrections should be taken into account based on the zeroth-order energy of the baryon, including the center-of-mass correction $\epsilon_{\text{c.m.}}$, the pion correction δM_B^{π}, and the gluon correction $(\Delta E_B)_g$ to generate the real baryon mass. The center-of-mass correction should be considered because of the translation invariance of baryons. The pion correction comes from the restoration of chiral symmetry of QCD theory. The gluon correction is generated by the short-range exchanging interaction among quarks. These three corrections are formulated in detail as follows [70,72,73].

The energy contribution of center-of-mass correction can be written as

$$\epsilon_{\text{c.m}} = e^{(1)}_{\text{c.m}} + e^{(2)}_{\text{c.m}}, \tag{9}$$

where

$$e^{(1)}_{\text{c.m.}} = \sum_{i=1}^{3}\left[\frac{m_{q_i}}{\sum_{k=1}^{3} m_{q_k}}\frac{6}{r_{0q_i}^2(3\epsilon'_{q_i}+m'_{q_i})}\right],$$

$$e^{(2)}_{\text{c.m.}} = \frac{1}{2}\Bigg[\frac{2}{\sum_k m_{q_k}}\sum_i a_i m_i\langle r_i^2\rangle + \frac{2}{\sum_k m_{q_k}}\sum_i a_i m_i\langle\gamma^0(i) r_i^2\rangle - \frac{3}{\left(\sum_k m_{q_k}\right)^2}\sum_i a_i m_i^2\langle r_i^2\rangle - \frac{1}{\left(\sum_k m_{q_k}\right)^2}\sum_i\langle\gamma^0(1) a_i m_i^2 r_i^2\rangle$$
$$- \frac{1}{\left(\sum_k m_{q_k}\right)^2}\sum_i\langle\gamma^0(2) a_i m_i^2 r_i^2\rangle - \frac{1}{\left(\sum_k m_{q_k}\right)^2}\sum_i\langle\gamma^0(3) a_i m_i^2 r_i^2\rangle\Bigg]. \tag{10}$$

The expectation values associated with the radii are evaluated as follows:

$$\langle r_i^2\rangle = \frac{(11\epsilon'_{qi}+m'_{qi})r_{0qi}^2}{2(3\epsilon'_{qi}+m'_{qi})},$$
$$\langle\gamma^0(i) r_i^2\rangle = \frac{(\epsilon'_{qi}+11m'_{qi})r_{0qi}^2}{2(3\epsilon'_{qi}+m'_{qi})},$$
$$\langle\gamma^0(i) r_j^2\rangle_{i\neq j} = \frac{(\epsilon'_{qi}+3m'_{qi})\langle r_j^2\rangle}{3\epsilon'_{qi}+m'_{qi}}. \tag{11}$$

The energy contributions of pion correction for nucleon and charmed baryons Λ_c^+, Σ_c^+, Ξ_{cc}^{++} are given by

$$\delta M_N^{\pi} = -\frac{171}{25} f_{NN\pi}^2 I_{\pi},$$
$$\delta M_{\Lambda_c^+}^{\pi} = -\frac{108}{25} f_{NN\pi}^2 I_{\pi},$$
$$\delta M_{\Sigma_c^+}^{\pi} = -\frac{12}{5} f_{NN\pi}^2 I_{\pi}, \tag{12}$$
$$\delta M_{\Xi_{cc}^{++}}^{\pi} = -\frac{27}{25} f_{NN\pi}^2 I_{\pi},$$

where

$$I_{\pi} = \frac{1}{\pi m_{\pi}^2}\int_0^{\infty} dk \frac{k^4 u^2(k)}{w_k^2}, \tag{13}$$

and the axial vector nucleon form factor is written as

$$u(k) = \left[1 - \frac{3}{2}\frac{k^2}{\lambda_u(5\epsilon'_u+7m'_u)}\right]e^{-\frac{1}{4}r_{0u}^2 k^2}. \tag{14}$$

The pseudovector $N\pi$ coupling constant $f_{NN\pi}$ can be derived from the Goldberg-Triemann relation,

$$f_{NN\pi} = \frac{25\epsilon'_u+35m'_u}{27\epsilon'_u+9m'_u}\frac{m_{\pi}}{4\sqrt{\pi}f_{\pi}}, \tag{15}$$

where $m_{\pi} = 140$ MeV and $f_{\pi} = 93$ MeV are the pion mass and the phenomenological pion decay constant, respectively.

The energy contribution from gluon correction in baryon mass consists of a color electric part and a magnetic part as

$$(\Delta E_B)_g = (\Delta E_B)_g^E + (\Delta E_B)_g^M, \tag{16}$$

where

$$(\Delta E_B)_g^E = \frac{1}{8\pi}\sum_{i,j}\sum_{a=1}^{8}\int\frac{d^3r_i d^3r_j}{|\vec{r}_i-\vec{r}_j|}\langle B|J_i^{0a}(\vec{r}_i)J_j^{0a}(\vec{r}_j)|B\rangle, \tag{17}$$

and

$$(\Delta E_B)_g^M = -\frac{1}{8\pi}\sum_{i,j}\sum_{a=1}^{8}\int\frac{d^3r_i d^3r_j}{|\vec{r}_i-\vec{r}_j|}\langle B|\vec{J}_i^a(\vec{r}_i)\cdot\vec{J}_j^a(\vec{r}_j)|B\rangle. \tag{18}$$

Here $J_i^{\mu a}(x)$ is the color current density of the ith quark,

$$J_i^{\mu a}(x) = g_c\overline{\psi}_q(x)\gamma^{\mu}\lambda_i^a\psi_q(x), \tag{19}$$

where λ_i^a are Gell-Mann SU(3) matrices and $\alpha_c = g_c^2/4\pi$. Here, we assume that the three quarks in charmed baryons retain the SU(3) symmetry, which is the same case for the strangeness baryons. Then, the color electric contribution and the color magnetic contribution can be given as

$$(\Delta E_B)_g^E = \alpha_c\left(b_{uu}I_{uu}^E + b_{uc}I_{uc}^E + b_{cc}I_{cc}^E\right), \tag{20}$$

and

$$(\Delta E_B)_g^M = \alpha_c\left(a_{uu}I_{uu}^M + a_{uc}I_{uc}^M + a_{cc}I_{cc}^M\right). \tag{21}$$

In Table I, the coefficients a_{ij} and b_{ij} are shown, which are related to the expectation values of spin and isospin operators from color current density in Eqs. (17) and (18) and are dependent on the species of baryon. They are obtained from

TABLE I. The numerical coefficients a_{ij} and b_{ij} are used to calculate the energy contributions of gluon correction for nucleon and charmed baryon masses.

Baryon	a_{uu}	a_{uc}	a_{cc}	b_{uu}	b_{uc}	b_{cc}
N	−3	0	0	0	0	0
Λ_c^+	−3	0	0	1	−2	1
Σ_c^+	1	−4	0	1	−2	1
Ξ_{cc}^{++}	0	−4	1	1	−2	1

the simplified form of Eqs. (17) and (18),

$$
\begin{aligned}
(\Delta E_B)_g^E &= \alpha_c \sum_{i,j} \left\langle \sum_a \lambda_i^a \lambda_j^a \right\rangle \frac{1}{\sqrt{\pi} R_{ij}} \\
&\quad \times \left[1 - \frac{\alpha_i + \alpha_j}{R_{ij}^2} + \frac{3\alpha_i \alpha_j}{R_{ij}^4} \right], \\
(\Delta E_B)_g^M &= \alpha_c \sum_{i<j} \left\langle \sum_a \lambda_i^a \lambda_j^a \sigma_i \cdot \sigma_j \right\rangle \\
&\quad \times \frac{32}{3\sqrt{\pi} R_{ij}^3} \frac{1}{(3\epsilon_i' + m_i')} \frac{1}{(3\epsilon_j' + m_j')},
\end{aligned} \tag{22}
$$

and the properties of Gell-Mann SU(3) matrices,

$$
\left\langle \sum_a (\lambda_i^a)^2 \right\rangle = \frac{16}{3}, \quad \left\langle \sum_a \lambda_i^a \lambda_j^a \right\rangle_{i \neq j} = -\frac{8}{3}. \tag{23}
$$

Therefore, the quantities I_{ij}^E and I_{ij}^M are given in the following equations,

$$
\begin{aligned}
I_{ij}^E &= \frac{16}{3\sqrt{\pi}} \frac{1}{R_{ij}} \left[1 - \frac{\alpha_i + \alpha_j}{R_{ij}^2} + \frac{3\alpha_i \alpha_j}{R_{ij}^4} \right], \\
I_{ij}^M &= \frac{256}{9\sqrt{\pi}} \frac{1}{R_{ij}^3} \frac{1}{(3\epsilon_i' + m_i')} \frac{1}{(3\epsilon_j' + m_j')},
\end{aligned} \tag{24}
$$

with

$$
\begin{aligned}
R_{ij}^2 &= 3 \left[\frac{1}{(\epsilon_i'^2 - m_i'^2)} + \frac{1}{(\epsilon_j'^2 - m_j'^2)} \right], \\
\alpha_i &= \frac{1}{(\epsilon_i' + m_i')(3\epsilon_i' + m_i')}.
\end{aligned} \tag{25}
$$

After all the above energy corrections are included, the mass of a charmed baryon in nuclear medium is expressed as

$$
M_B^* = E_B^{*0} - \epsilon_{\text{c.m.}} + \delta M_B^{\pi} + (\Delta E_B)_g^E + (\Delta E_B)_g^M. \tag{26}
$$

Then, the Λ_c^+ hypernuclei will be studied in the QMF model. A single-Λ_c^+ hypernucleus is regarded as a binding system of a Λ_c^+ baryon and many nucleons which interact via exchanging σ, ω, and ρ mesons. This mechanism of baryon-baryon interaction is originated from the RMF model. Therefore, the Lagrangian of QMF model for Λ_c^+ hypernucleus can be written as an analogous form in the RMF model [30,38,73],

$$
\begin{aligned}
\mathcal{L}_{\text{QMF}} &= \overline{\psi}_N \Big[i\gamma^\mu \partial_\mu - M_N^* - g_{\omega N} \omega_\mu \gamma^\mu - g_{\rho N} \rho_{\alpha\mu} \tau_\alpha \gamma^\mu \\
&\quad - e \frac{(1 - \tau_3)}{2} A_\mu \gamma^\mu \Big] \psi_N \\
&\quad + \overline{\psi}_{\Lambda_c^+} \Big[i\gamma^\mu \partial_\mu - M_{\Lambda_c^+}^* - g_{\omega \Lambda_c^+} \omega_\mu \gamma^\mu \\
&\quad + \frac{f_{\omega \Lambda_c^+}}{2M_{\Lambda_c^+}} \sigma^{\mu\nu} \partial_\nu \omega_\mu - e q_{\Lambda_c^+} A_\mu \gamma^\mu \Big] \psi_{\Lambda_c^+} \\
&\quad + \frac{1}{2} \partial_\mu \sigma \partial^\mu \sigma - \frac{1}{2} m_\sigma^2 \sigma^2 - \frac{1}{3} g_2 \sigma^3 - \frac{1}{4} g_3 \sigma^4 \\
&\quad - \frac{1}{4} \Omega_{\mu\nu} \Omega^{\mu\nu} + \frac{1}{2} m_\omega^2 \omega_\mu \omega^\mu + \frac{1}{4} c_3 \left(\omega_\mu \omega^\mu \right)^2 \\
&\quad - \frac{1}{4} R_{\alpha\mu\nu} R_\alpha^{\mu\nu} + \frac{1}{2} m_\rho^2 \rho_{\alpha\mu} \rho_\alpha^\mu - \frac{1}{4} F_{\mu\nu} F^{\mu\nu},
\end{aligned} \tag{27}
$$

with

$$
\begin{aligned}
\Omega_{\mu\nu} &= \partial_\mu w_\nu - \partial_\nu w_\mu, \\
R_{\alpha\mu\nu} &= \partial_\mu \rho_{\alpha\nu} - \partial_\nu \rho_{\alpha\mu}, \\
F_{\mu\nu} &= \partial_\mu A_\nu - \partial_\nu A_\mu.
\end{aligned} \tag{28}
$$

ψ_N and $\psi_{\Lambda_c^+}$ are the nucleon and Λ_c^+ baryon fields, respectively. A_μ is the electricmagnetic field for the Coulomb interaction between charged baryons. M_N^* and $M_{\Lambda_c^+}^*$ are the effective masses of nucleon and Λ_c^+, which can be obtained from the quark potential model. These effective masses are strongly relevant to the magnitudes of σ meson in the RMF model. The coupling constants between ω, ρ mesons and nucleons, $g_{\omega N}$ and $g_{\rho N}$, can be determined by the naive quark counting rules, $g_{\omega N} = 3g_{\omega q}$ and $g_{\rho N} = g_{\rho q}$. $g_{\omega q}$ and $g_{\rho q}$ are fixed by the ground-state properties of several doubly magic nuclei. The determination of coupling constants between the ω meson and the Λ_c^+ baryon, $g_{\omega \Lambda_c^+}$ and $f_{\omega \Lambda_c^+}$, will be discussed in the next section. α denotes the index of isospin vector. $q_{\Lambda_c^+}$ is the charge of the Λ_c^+ baryon with the unit charge e. The nonlinear terms of σ and ω mesons are included in this Lagrangian, which can largely improve the descriptions of properties of finite nuclei [72]. In this work, the tensor coupling between the ω meson and the Λ_c^+ baryon, $\frac{f_{w\Lambda_c^+}}{2M_{\Lambda_c^+}} \sigma^{\mu\nu} \partial_\nu \omega_\mu$, is also introduced following the conventional scheme for Λ hypernuclei, where the spin-orbit splittings were very small from the experimental observations [28–30].

In this work, the charmed hypernuclei are regarded as the spherical nuclei and the time-reversal symmetry is assumed. Therefore only time components of the ω, ρ, and A fields exist. Furthermore, there is not any contribution from baryon currents. For convenience, ω_0, ρ_0, and A_0 will be replaced by ω, ρ, and A in the following. Because of charge conservation, only the third component of the isospin vectors provides a nonvanishing contribution. Here, $\tau_3 = -1$ for proton and $\tau_3 = 1$ for neutron are defined in conventional calculations. With the mean-field approximation, we can get the equations of motion of baryons and mesons by using the Euler-Lagrange

TABLE II. The potential parameters a_q and V_q for u and c quarks corresponding to $m_u = 250$ MeV as set A, $m_u = 300$ MeV as set B, and $m_u = 350$ MeV as set C.

	m_u (MeV)	V_u (MeV)	a_u (fm^{-3})	m_c (MeV)	V_c (MeV)	a_c (fm^{-3})
Set A	250	−24.286601	0.579450	1300	284.58724	0.118172
Set B	300	−62.257187	0.534296	1350	239.53994	0.117312
Set C	350	−102.041575	0.495596	1400	193.67265	0.116036

equation. The Dirac equations for baryons are given as

$$\left[i\gamma^\mu\partial_\mu - M_N^* - g_{\omega N}\omega\gamma^0 - g_{\rho N}\rho\tau_3\gamma^0 - e\frac{(1-\tau_3)}{2}A\gamma^0\right] \times \psi_N = 0,$$
$$\left[i\gamma^\mu\partial_\mu - M_{\Lambda_c^+}^* - g_{\omega\Lambda_c^+}\omega\gamma^0 + \frac{f_{\omega\Lambda_c^+}}{2M_{\Lambda_c^+}}\sigma^{0i}\partial_i\omega - eq_{\Lambda_c^+}A\gamma^0\right] \times \psi_{\Lambda_c^+} = 0. \quad (29)$$

The equations of motion for mesons can be obtained by

$$\Delta\sigma - m_\sigma^2\sigma - g_2\sigma^2 - g_3\sigma^3 = \frac{\partial M_N^*}{\partial\sigma}\langle\overline{\psi}_N\psi_N\rangle + \frac{\partial M_{\Lambda_c^+}^*}{\partial\sigma}\langle\overline{\psi}_{\Lambda_c^+}\psi_{\Lambda_c^+}\rangle,$$
$$\Delta\omega - m_\omega^2\omega - c_3\omega^3 = -g_{\omega N}\langle\overline{\psi}_N\gamma^0\psi_N\rangle - g_{\omega\Lambda_c^+}\langle\overline{\psi}_{\Lambda_c^+}\gamma^0\psi_{\Lambda_c^+}\rangle + \frac{f_{\omega\Lambda_c^+}}{2m_{\Lambda_c^+}}\partial_i\langle\overline{\psi}_{\Lambda_c^+}\sigma^{0i}\psi_{\Lambda_c^+}\rangle,$$
$$\Delta\rho - m_\rho^2\rho = -g_{\rho N}\langle\overline{\psi}_N\tau_3\gamma^0\psi_N\rangle,$$
$$\Delta A = -e\left\langle\overline{\psi}_N\frac{(1-\tau_3)}{2}\gamma^0\psi_N\right\rangle - e\langle\overline{\psi}_{\Lambda_c^+}q_{\Lambda_c^+}\gamma^0\psi_{\Lambda_c^+}\rangle. \quad (30)$$

These equations can be solved self-consistently within numerical methods to generate the single-particle energies of baryons and the total energy of charmed hypernucleus.

III. RESULT AND DISCUSSION

A. Properties of baryons

The potential parameters a_q and V_q for u, d, and c quarks should be first fixed to investigate the properties of baryons. u and d quarks are considered equally because of the very small differences of properties between them, while the c quark is distinguished from them, whose mass is very large. The u or d quark mass in the QMF model is adopted from 250–350 MeV as constituent quark [72,73]. Therefore, to discuss the influence of quark mass on the properties of baryons, the constituent quark mass for u quark or d quark is taken as 250, 300, and 350 MeV, respectively, in this work. The corresponding potential parameters a_u and V_u can be derived by fitting the mass and radius of the free nucleon, which have been obtained in our previous work [72,73]. For the charm c quark, its mass is chosen as 1300, 1350, and 1400 MeV, correspondingly now. The potential parameters a_c and V_c are gained by fitting the experimental masses of Λ_c^+, Σ_c^+, and Ξ_{cc}^{++} baryons in free space [41] with the least-squares method.

These parameters are listed in Table II. For the convenience of latter discussion, the parameters corresponding to $m_u = 250$ MeV in Table II are named as set A, the parameters corresponding to $m_u = 300$ MeV as set B, and the parameter corresponding to $m_u = 350$ MeV as set C.

The masses of charmed baryons, Λ_c^+, Σ_c^+, and Ξ_{cc}^{++} in free space generated by set A, set B, and set C are listed to compare with the latest experimental data [41] in Table III. Meanwhile, the contributions from center-of-mass correction, pion correction, and gluon correction to the masses of charmed baryons

TABLE III. The masses of charmed baryons (Λ_c^+, Σ_c^+, and Ξ_{cc}^{++}) in free space with set A, set B, and set C parameter sets, compared with the experimental data and various contributions in charmed baryon masses, respectively (the units of all quantities are MeV).

	Baryon	E_B^0	$\epsilon_{\rm cm}$	δM_B^π	$(\Delta E_B)g$	$M_B^{\rm Theor.}$	$M_B^{\rm Expt.}$[41]
Set A	Λ_c^+	2562.949	137.904	−65.172	−47.747	2312.126	2286.46 ± 0.14
	Σ_c^+	2562.949	137.904	−36.207	−0.790	2388.048	2452.9 ± 0.4
	Ξ_{cc}^{++}	3737.473	96.999	−16.293	−15.607	3608.574	3621.40 ± 0.72 ± 0.27 ± 0.14
Set B	Λ_c^+	2558.524	140.641	−69.277	−43.096	2305.510	2286.46 ± 0.14
	Σ_c^+	2558.524	140.641	−38.487	−1.291	2378.105	2452.9 ± 0.4
	Ξ_{cc}^{++}	3741.683	97.896	−17.319	−14.588	3611.879	3621.40 ± 0.72 ± 0.27 ± 0.14
Set C	Λ_c^+	2553.749	141.522	−72.829	−39.007	2300.390	2286.46 ± 0.14
	Σ_c^+	2553.749	141.522	−40.461	−1.674	2370.092	2452.9 ± 0.4
	Ξ_{cc}^{++}	3744.384	98.099	−18.207	−13.640	3614.437	3621.40 ± 0.72 ± 0.27 ± 0.14

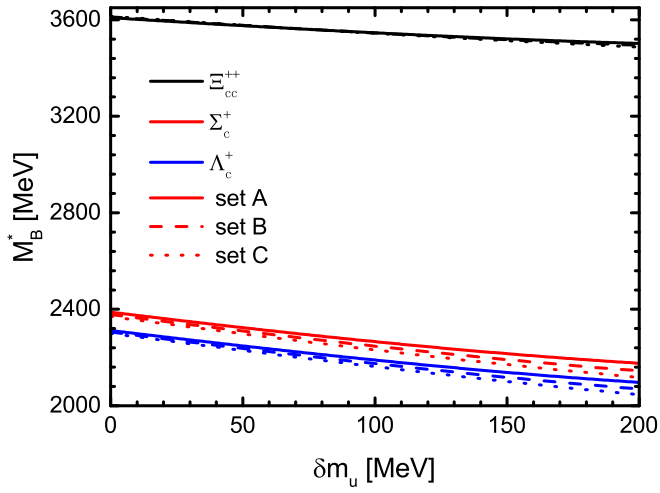

FIG. 1. The effective masses of charmed baryons M_B^* for Λ_c^+, Σ_c^+, and Ξ_{cc}^{++} as functions of the quark mass corrections δm_u with three parameter sets [set A (solid curves), set B (dashed curves), and set C (dotted curves)].

are also shown. It can be found that the charmed baryon masses from the quark potential model almost reproduce their experimental data [41] with errors less than 5% because there are only two degrees of freedom in the confinement potential, V_c and a_c. Furthermore, the masses of Ξ_{cc}^{++} from these three sets reproduce the experimental data better comparing to other two baryons. It is because two c quarks provide their contributions to Ξ_{cc}^{++}, which is more sensitive to the strengths a_c and V_c in the confinement potentials.

The mass of baryon in the nuclear medium M_B^* will vary with nucleon density, because the properties of baryons in the nuclear many-body system are influenced by the surrounding baryons as the famous EMC effect [75]. In the QMF model, such medium effect is included through the effective quark mass depending on the σ meson field. In the charmed hypernucleus, the σ field only couples with u and d quarks. Therefore, the coupling constant between the σ meson and c quark should be taken as zero so that the effective masses of charmed baryons are only affected by u and d quarks. The effective baryon masses are the functions of quark mass corrections $\delta m_u = m_u - m_u^* = g_{\sigma u}\sigma$. In Fig. 1, the effective masses of charmed baryons, Λ_c^+, Σ_c^+, and Ξ_{cc}^{++}, as functions of u quark mass correction δm_q for different parameter sets are plotted. It is found that the effective baryon masses decreased with δm_q increasing from the EMC effect of surrounding baryons. When δm_q is zero, the effective masses of these charmed baryons correspond to the free baryon masses. With δm_q increasing, the differences of effective masses of Λ_c^+ and Σ_c^+ baryons among parameter sets A, B, and C are more obvious than those of the Ξ_{cc}^{++} baryon. The reason is that comparing with the Ξ_{cc}^{++} hyperon, there are two light quarks contained in Λ_c^+ and Σ_c^+ baryons, which are influenced more by the σ meson. It is very similar to the results of Λ, Σ, and Ξ hyperons in our previous work [73].

B. Properties of Λ_c^+ hypernuclei

The properties of Λ_c^+ hypernuclei can be studied within the QMF model, once the relation between quark mass corrections and effective masses of charmed Λ_c^+ baryons are derived from the quark potential model. The coupling constants between mesons and nucleons have been determined by fitting the ground-state properties of several doubly magic nuclei in our previous work, i.e., the binding energies per nucleon and the charge radii of ^{40}Ca, ^{48}Ca, ^{90}Zr, and ^{208}Pb [72,73]. The χ^2 function was defined as

$$\chi^2 = \frac{1}{N}\sum_{i=1}^{N}\left(\frac{X_i^{\text{Theo.}} - X_i^{\text{Exp.}}}{X_i^{\text{Exp.}}}\right)^2, \tag{31}$$

with the least square method, where X represents the binding energy, E/A, and charge radius r_{ch} of nuclei. To discuss the mass influences of constituent quark, there were three masses of u, d quark adopted as 250, 300, 350 MeV. The corresponding coupling constants between mesons and nucleon were named as QMF-NK1, QMF-NK2, and QMF-NK3, respectively. Their corresponding χ^2 were 3.42×10^{-5}, 2.33×10^{-5}, and 1.08×10^{-5}. These parameters are listed in Table IV for the later discussions conveniently.

The isospin of the Λ_c^+ baryon is zero, which does not interact with the isovector ρ meson. On the other hand, the coupling strength between the σ meson and Λ_c^+ was included in the effective mass of the Λ_c^+ baryon. Therefore, the $\Lambda_c^+ N$ potential is mainly dependent on the coupling constant between the ω meson and the Λ_c^+ baryon, $g_{\omega\Lambda_c^+}$, in the QMF model. However, there is no specific information about the $\Lambda_c^+ N$ interaction at the aspect of experiment. Therefore, we would like to adopt two schemes to fix $g_{\omega\Lambda_c^+}$. The first way is following the method of the QMC model and the RMF model [47–49,51,52], where $g_{\omega\Lambda_c^+} = 2/3 g_{\omega N}$ according to the naive quark counting rule. In our previous work [72], the coupling strength between ω meson and nucleon, $g_{\omega N}$, took three values, which were dependent on constituent quark masses. For the convenience of later discussion, the corresponding values of $g_{\omega\Lambda_c^+}$ from the naive quark counting rule are called QMF-NK1C, QMF-NK2C, and QMF-NK3C, respectively.

Furthermore, the $\Lambda_c^+ N$ potentials were simulated by the lattice QCD method with different pion masses recently, where the magnitude of the $\Lambda_c^+ N$ potential in heavy nuclei,

TABLE IV. The coupling constants between mesons and nucleon in QMF-NK1, QMF-NK2, and QMF-NK3 sets.

	g_σ^q	g_ω	g_ρ	g_2 (fm^{-1})	g_3	c_3
QMF-NK1	5.15871	11.54726	3.79601	−3.52737	−78.52006	305.00240
QMF-NK2	5.09346	12.30084	4.04190	−3.42813	−57.68387	249.05654
QMF-NK3	5.01631	12.83898	4.10772	−3.29969	−39.87981	221.68240

TABLE V. The coupling constants between ω meson and Λ_c^+ from the naive quark counting rule and lattice QCD simulation.

	QMF-NK1C	QMF-NK2C	QMF-NK3C	QMF-NK1C′	QMF-NK2C′	QMF-NK3C′
$g_{\omega\Lambda_c^+}$	7.69817	8.20056	8.55932	9.16621	9.60204	9.93609

$^{209}_{\Lambda_c^+}$Pb, was just one-half of the ΛN potential at the central region by employing the single-folding potential method [65]. Based on this achievement, we also would like to determine $g_{\omega\Lambda_c^+}$ with the following scheme. First, we make an approximation that the binding energy of Λ_c^+ in $^{209}_{\Lambda_c^+}$Pb is one-half of that in $^{209}_{\Lambda}$Pb in the QMF model when the Coulomb contribution is turned off. Then the single-Λ binding energies at the $1s$ state in $^{209}_{\Lambda}$Pb are calculated within the parameters from our previous work in Ref. [73]. Now the $g_{\omega\Lambda_c^+}$ can be determined through fitting the single-Λ_c^+ binding energy of $^{209}_{\Lambda_c^+}$Pb. Finally, three coupling constants between ω meson and Λ_c^+ are obtained, which are $g_{\omega\Lambda_c^+} = 0.7938 g_{\omega N}$ for QMF-NK1C′, $g_{\omega\Lambda_c^+} = 0.7806 g_{\omega N}$ for QMF-NK2C′, and $g_{\omega\Lambda_c^+} = 0.7739 g_{\omega N}$ for QMF-NK3C′. In the QMF or RMF model, the single-baryon potential can be written as $U_B = U_S^B + U_V^B$. The scalar and vector potentials, U_S^B and U_V^B, are related to the scalar meson and vector mesons, respectively. In the QMF model, the scalar component was decided by the quark level. Therefore, when the single-baryon potential is well known, the strength of the vector potential is easily obtained. Although the present lattice QCD simulation only included the contributions from $^1S_0$ and $^3S_1 - ^3D_1$ channels, they can already represent the basic characters of $\Lambda_c^+ N$ potentials. It should be a good attempt to connect the density functional theory and lattice calculations with the single-baryon potential. The tensor coupling between the ω meson and the Λ_c^+ baryon will be also included to generate a small spin-orbit splitting in hypernucleus following the conventional way, $f_{\omega\Lambda_c^+} = -g_{\omega\Lambda_c^+}$ [28–30]. The detailed values of $g_{\omega\Lambda_c^+}$ from these two schemes are listed in Table V.

It can be found that these coupling constants between the ω meson and the Λ_c^+ baryon are larger than that generated from the SU(4) symmetry in meson-exchange potential [68], where $g_{\omega\Lambda_c^+}$ is 5.28191. It is because the coupling strengths between the scalar meson and the Λ_c^+ baryon in the QMF model are relatively stronger.

The binding energies per baryon and various radius of single-Λ_c^+ hypernuclei are shown in Table VI within QMF-NK3C and QMF-NK3C′ sets from light to heavy mass systems, when the Λ_c^+ baryon occupies the lowest $1s_{1/2}$ state. The corresponding properties of normal nuclei as the core of the single-Λ_c^+ hypernuclei are also give as comparison. With the QMF-NK3C set, the nuclear many-body system becomes more bound when the Λ_c^+ baryon is included and its charge radius, proton radius, and neutron radius slightly increase. However, the radii of Λ_c^+ baryon density distribution are smaller than those of the proton and neutron in such a case. It demonstrates that the Λ_c^+ baryon is attracted inside the nuclei. These calculations are consistent with the results from the RMF model by Tan *et al.* [51]. While there are only bound states between the Λ_c^+ baryon and normal nuclei core up to $^{52}_{\Lambda_c^+}$V for single-Λ_c^+ hypernuclei within the QMF-NK3C′ set, where the coupling constant between the ω meson and the Λ_c^+ baryon is larger than that in the QMF-NK3C set. It generates a more repulsive $\Lambda_c^+ N$ potential. Furthermore, Coulomb contributions between the Λ_c^+ baryon and protons are growing with the mass number A. Therefore, it can be easily understood that there is no heavy-Λ_c^+ hypernuclei when the $\Lambda_c^+ N$ potential is not so attractive. Actually, this conclusion is very similar to recent work by Miyamoto *et al.*, where the $\Lambda_c^+ N$ poten-

TABLE VI. Binding energies per baryon $-E/A$, charge radius $r_{\rm ch}$, and radius (in fm) of protons r_p, neutrons r_n, and Λ_c^+ baryon $r_{\Lambda_c^+}$, in $\Lambda_c^+(1s_{1/2})$ with QMF-NK3C and QMF-NK3C′ sets for ^{16}O, ^{40}Ca, ^{51}V, ^{89}Y, ^{139}La, and ^{208}Pb and their corresponding single Λ_c^+ hypernuclei.

	QMF-NK3C					QMF-NK3C′				
	$-E/A$	$r_{\rm ch}$	r_p	r_n	$r_{\Lambda_c^+}$	$-E/A$	$r_{\rm ch}$	r_p	r_n	$r_{\Lambda_c^+}$
^{16}O	8.1377	2.7225	2.6042	2.5763		8.1377	2.7225	2.6042	2.5763	
$^{17}_{\Lambda_c^+}$O	9.1039	2.7298	2.6118	2.5797	1.8199	7.7937	2.7418	2.6244	2.5936	3.1746
^{40}Ca	8.5916	3.4562	3.3638	3.3141		8.5916	3.4562	3.3638	3.3141	
$^{41}_{\Lambda_c^+}$Ca	9.0333	3.4630	3.3708	3.3174	2.2599	8.4159	3.4692	3.3771	3.3252	3.8017
^{51}V	8.6403	3.6050	3.5200	3.6127		8.6403	3.6050	3.5200	3.6127	
$^{52}_{\Lambda_c^+}$V	9.0162	3.6086	3.5237	3.6123	2.3773	8.5047	3.6190	3.5343	3.6246	3.7366
^{89}Y	8.6990	4.2435	4.1724	4.2923		8.6990	4.2435	4.1724	4.2923	
$^{90}_{\Lambda_c^+}$Y	8.8925	4.2466	4.1755	4.2921	2.9105					
^{139}La	8.4276	4.8556	4.7954	4.9826		8.4276	4.8556	4.7954	4.9826	
$^{140}_{\Lambda_c^+}$La	8.5388	4.8565	4.7964	4.9812	3.5325					
^{208}Pb	7.8992	5.5037	5.4517	5.6898		7.8992	5.5037	5.4517	5.6898	
$^{209}_{\Lambda_c^+}$Pb	7.9623	5.5052	5.4532	5.6892	4.2618					

TABLE VII. Energy levels (in MeV) of Λ_c^+ hyperons for ${}^{17}_{\Lambda_c^+}$O, ${}^{41}_{\Lambda_c^+}$Ca, ${}^{52}_{\Lambda_c^+}$V, ${}^{140}_{\Lambda_c^+}$La, and ${}^{209}_{\Lambda_c^+}$Pb with QMF-NK3C and QMF-NK3C′ sets.

	QMF-NK3C					QMF-NK3C′				
	${}^{17}_{\Lambda_c^+}$O	${}^{41}_{\Lambda_c^+}$Ca	${}^{52}_{\Lambda_c^+}$V	${}^{140}_{\Lambda_c^+}$La	${}^{209}_{\Lambda_c^+}$Pb	${}^{17}_{\Lambda_c^+}$O	${}^{41}_{\Lambda_c^+}$Ca	${}^{52}_{\Lambda_c^+}$V	${}^{140}_{\Lambda_c^+}$La	${}^{209}_{\Lambda_c^+}$Pb
$1s_{1/2}$	−24.3013	−25.8621	−27.2769	−21.8919	−18.0800	−1.9540	−0.5425	−0.6116		
$1p_{3/2}$	−16.0223	−20.4776	−22.4005	−19.7552	−16.6644					
$1p_{1/2}$	−15.9654	−20.4470	−22.3784	−19.7470	−16.6568					
$1d_{5/2}$	−7.4825	−14.2550	−16.6196	−16.8628	−14.5743					
$1d_{3/2}$	−7.3925	−14.1977	−16.5734	−16.8451	−14.5595					
$1f_{7/2}$		−7.5936	−10.3256	−13.3801	−11.9527					
$1f_{5/2}$		−7.5100	−10.2519	−13.3494	−11.9285					
$1g_{9/2}$		−0.7306	−3.7352	−9.4215	−8.8898					
$1g_{7/2}$		−0.6267	−3.6360	−9.3748	−8.8543					

tial from lattice simulations was folded to calculate the Λ_c^+ hypernuclei [65].

The energy levels of Λ_c^+ baryons at different angular momenta for various single charmed hypernuclei by using QMF-NK3C and QMF-NK3C′ sets are listed in detail in Table VII. The deepest single-Λ_c^+ energy level appears in ${}^{52}_{\Lambda_c^+}$V with the parameter set QMF-NK3C at a given angular momentum. It is generated by the competition between the Coulomb repulsion and attractive $\Lambda_c^+ N$ potential. Both of them become larger for heavy nuclei system. The contribution of the $\Lambda_c^+ N$ potential is stronger than that from Coulomb interaction for light hypernuclei, while this situation is the opposite at the large A case. This behavior was also shown in the works by Tan *et al.* [52] and Vidaña *et al.* [68]. The deepest energy levels of Λ_c^+ hypernuclei appeared in ${}^{41}_{\Lambda_c^+}$Ca from Tan *et al.* with the RMF model, while in model C of Ref. [68], the deepest energy level for the $1s$ state appeared in ${}^{91}_{\Lambda_c^+}$Zr. Its $\Lambda_c^+ N$ potential was not so attractive among three models.

It is also found that the spin-orbit splitting of Λ_c^+ hypernuclei is very small. In addition to the tensor coupling between ω and Λ_c^+, the mass of Λ_c^+ baryons also will influence the spin-orbit force of single-Λ_c^+ hypernuclei. When the Dirac equation related to the Λ_c^+ baryon is reduced to the corresponding Schrödinger equation, the spin-orbit force is inversely proportional to the Λ_c^+ baryon mass. Therefore, the spin-orbit force in Λ_c^+ hypernuclei is smaller than that in Λ hypernuclei and normal nuclei, which was consistent with results from the RMF model [52] and the perturbative many-body method [68]. On the other hand, the $\Lambda_c^+ N$ potential in QMF-NK3C′ is much smaller, where only the $1s_{1/2}$ state of Λ_c^+ can exist up to ${}^{52}_{\Lambda_c^+}$V.

In Fig. 2, the binding energies of single-Λ_c^+ hypernuclei at different angular momenta states are systematically calculated with QMF-NK1C, QMF-NK2C, and QMF-NK3C parameter sets. Their differences among three sets for light and heavy hypernuclei are very small. The differences become obvious at intermediate mass region. The spin-orbit forces of Λ_c^+ hypernuclei are very small now. Therefore, we did not distinguish the spin-orbit partners at a fixed orbital angular momentum here. The corresponding results from QMF-NK1C′, QMF-NK2C′, and QMF-NK3C′ sets are plotted in Fig. 3, where the Λ_c^+ only can occupy the $1s_{1/2}$ state. Furthermore, the

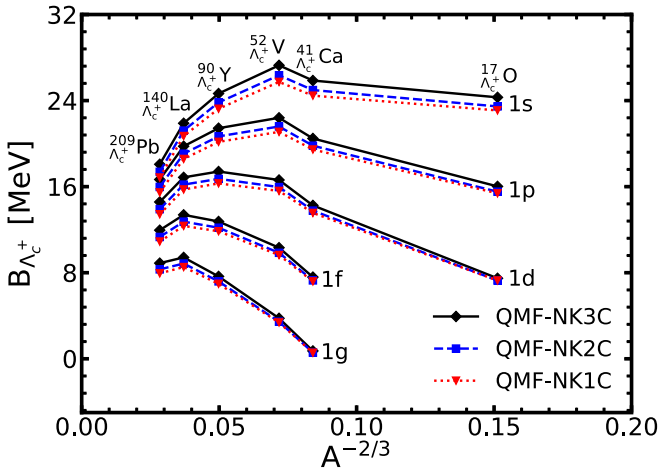

FIG. 2. The binding energies of single-Λ_c^+ hyperons at various angular momenta from ${}^{17}_{\Lambda_c^+}$O to ${}^{209}_{\Lambda_c^+}$Pb with three parameter sets [QMF-NK1C (dotted curve), QMF-NK2C (dashed curve), and QMF-NK3C (solid curve)].

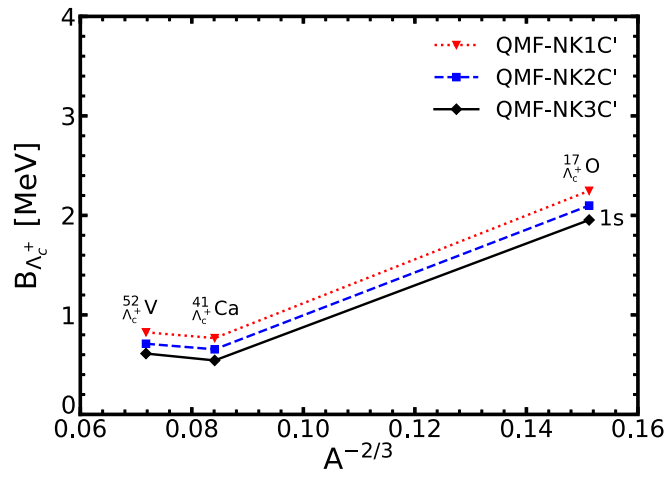

FIG. 3. The binding energies of single Λ_c^+ hyperons from ${}^{17}_{\Lambda_c^+}$O to ${}^{52}_{\Lambda_c^+}$V hypernuclei with three parameter sets [QMF-NK1C′ (dotted curve), QMF-NK2C′ (dashed curve), and QMF-NK3C′ (solid curve)].

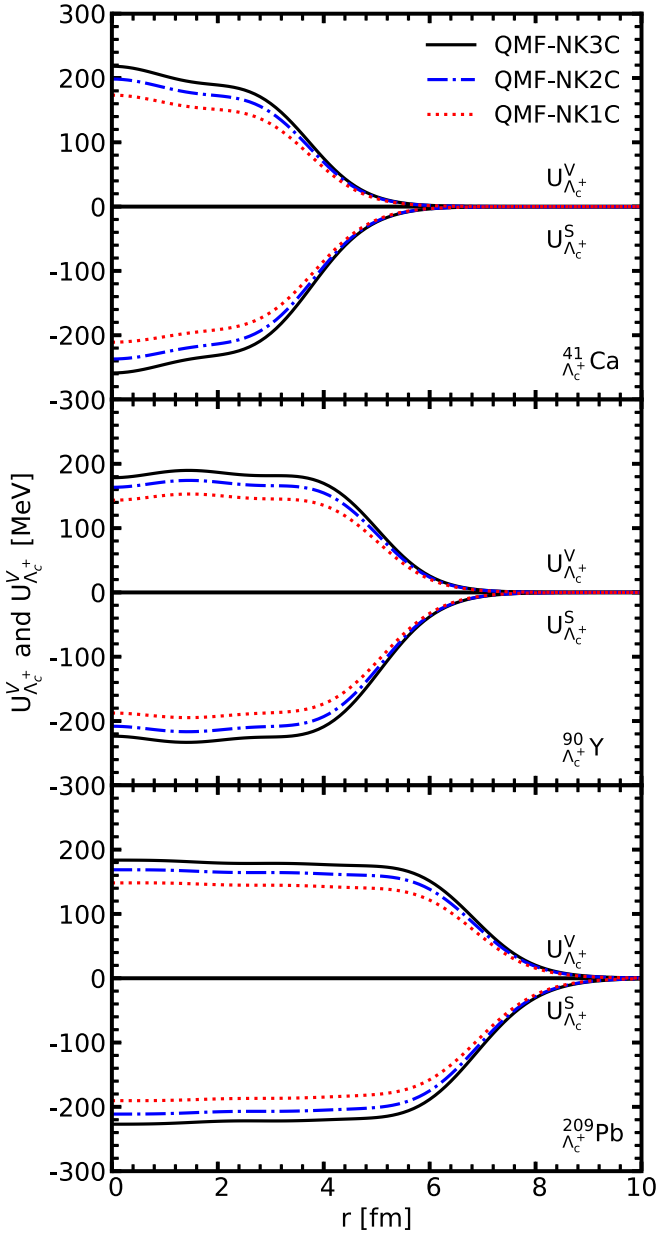

FIG. 4. The scalar potentials $U^S_{\Lambda_c^+}$ and vector potentials $U^V_{\Lambda_c^+}$ at Λ_c^+ in the $1s_{1/2}$ state for $^{41}_{\Lambda_c^+}$Ca, $^{90}_{\Lambda_c^+}$Y, and $^{209}_{\Lambda_c^+}$Pb with three parameter sets [QMF-NK1C (dotted curves), QMF-NK2C (dashed-dotted curves), and QMF-NK3C (solid curves)].

binding energies of Λ_c^+ hypernuclei in QMF-NK3C are the largest in the parameter sets which are determined by the naive quark counting rules, while from the lattice simulations, the QMF-NK3C′ set generates the smallest binding energies and the differences among the three sets of parameters are almost negligible. It is because the Λ_c^+N potentials from lattice simulations are fixed as one-half of ΛN potentials.

The scalar potentials $U^S_{\Lambda_c^+}$ and vector potentials $U^V_{\Lambda_c^+}$ of Λ_c^+ baryons at $1s_{1/2}$ states for $^{41}_{\Lambda_c^+}$Ca, $^{90}_{\Lambda_c^+}$Y, and $^{209}_{\Lambda_c^+}$Pb as functions of their radius are shown in Fig. 4 with QMF-NK1C, QMF-NK2C, and QMF-NK3C sets. These scalar and vector potentials are produced by the σ and ω mesons, respectively.

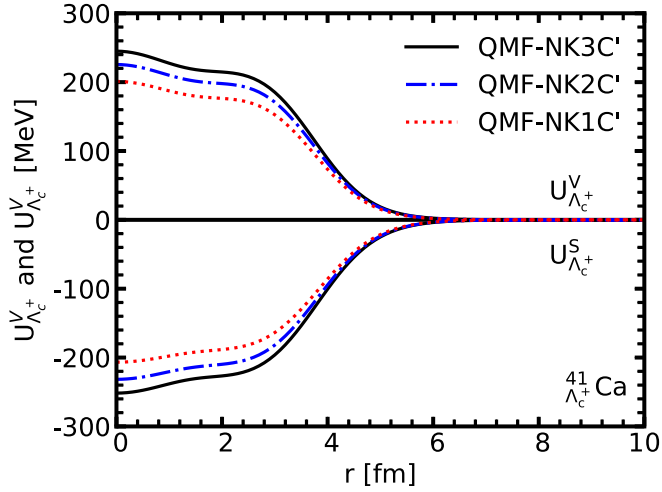

FIG. 5. The scalar potential $U^S_{\Lambda_c^+}$ and vector potential $U^V_{\Lambda_c^+}$ at Λ_c^+ in the $1s_{1/2}$ state for $^{41}_{\Lambda_c^+}$Ca with three parameter sets [QMF-NK1C′ (dotted curves), QMF-NK2C′ (dashed-dotted curves), and QMF-NK3C′ (solid curves)].

They have the similar magnitudes and lead to total attractive Λ_c^+N potentials to bind the Λ_c^+ hypernuclei. This attractive potential at $r = 0$ is about -40 MeV. The $U^S_{\Lambda_c^+}$ and $U^V_{\Lambda_c^+}$ have the largest magnitude from QMF-NK3C. This is because the effective Λ_c^+ mass in set C is the smallest, which can be expressed as $M^*_{\Lambda_c^+} = M_{\Lambda_c^+} + U^S_{\Lambda_c^+}$. The corresponding vector coupling constant $g_{\omega\Lambda_c^+}$ is the biggest. The ranges of scalar and vector potentials of Λ_c^+ baryon increase with the mass of Λ_c^+ hypernuclei. The scalar potential $U^S_{\Lambda_c^+}$ and vector potential $U^V_{\Lambda_c^+}$ from QMF-NK1C′, QMF-NK2C′, and QMF-NK3C′ for $^{41}_{\Lambda_c^+}$Ca are plotted in Fig. 5. Their behaviors are very similar to the QMF-NK1C, QMF-NK2C, and QMF-NK3C sets except the smaller vector potentials. In these cases, the $U^S_{\Lambda_c^+} + U^V_{\Lambda_c^+}$ are about -13 MeV at the central region of charmed hypernuclei, which generated the smaller binding energies.

Actually, the properties of Λ_c^+ baryons in Λ_c^+ hypernuclei are determined by the total potentials from the σ meson, the ω meson, and the Coulomb field. In Fig. 6, the contributions to Λ_c^+N potential from σ and ω, $V_\sigma + V_\omega$, the Coulomb interaction V_A, and the total $V_{\rm all} = V_\sigma + V_\omega + V_A$ are shown for $^{17}_{\Lambda_c^+}$O and $^{209}_{\Lambda_c^+}$Pb within the QMF-NK3C (left panel) and QMF-NK3C′ (right panel) sets. It can be found that the sums of σ and ω potentials for $^{17}_{\Lambda_c^+}$O and $^{209}_{\Lambda_c^+}$Pb both are around -45 MeV by using the QMF-NK3C set. However, the contributions provided by Coulomb force in these two hypernuclei are completely different, which are around 7 MeV and 26 MeV for $^{17}_{\Lambda_c^+}$O and $^{209}_{\Lambda_c^+}$Pb, respectively. Therefore, the total potential of $^{209}_{\Lambda_c^+}$Pb is much smaller than that of $^{17}_{\Lambda_c^+}$O, which generates the deeper single-Λ_c^+ energies for light charmed hypernuclei. In the QMF-NK3C′ set, there are also similar behaviors. Now, the $V_\sigma + V_\omega$ is just about -15 MeV. In this case, the strong repulsion from the Coulomb interaction cannot generate any bound state for heavy Λ_c^+ hypernuclei.

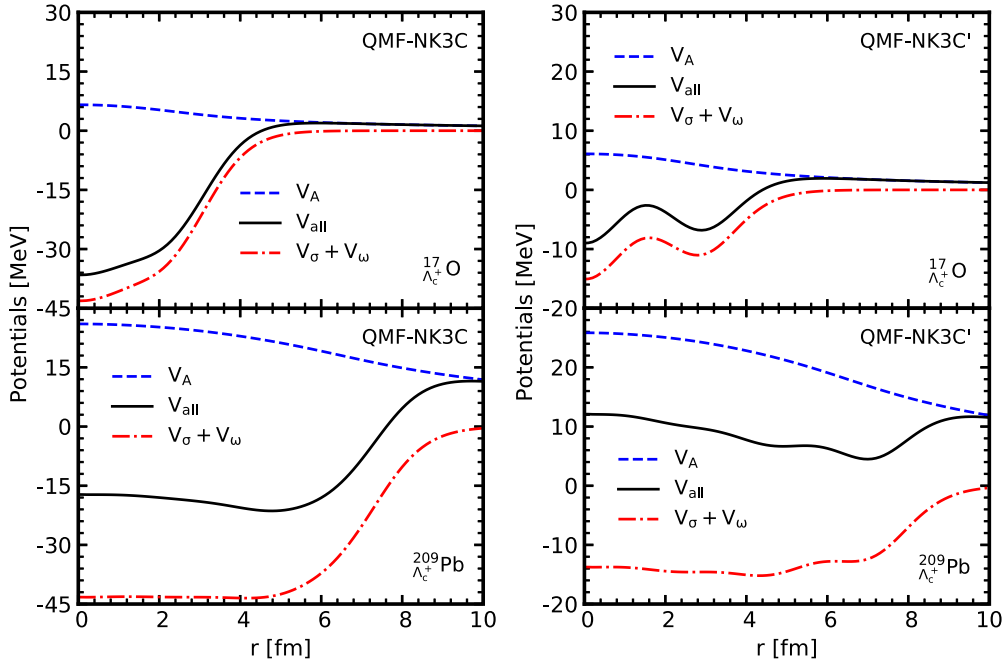

FIG. 6. The different contributions to the central potential $V_{\rm all} = V_A + V_\sigma + V_\omega$ for $^{17}_{\Lambda_c^+}$O and $^{209}_{\Lambda_c^+}$Pb within QMF-NK3C and QMF-NK3C'. The dashed lines are from the Coulomb contribution, the dashed-dotted curves represent the sum of contributions from σ meson and ω meson, and the total ones are given as solid curves.

IV. CONCLUSION

The single-Λ_c^+ hypernuclei were studied within the quark mean-field (QMF) model. First, a baryon was regarded as a combination composed by three constituent quarks, which were confined by central harmonics oscillator potentials with the Dirac vector-scalar mixing form. Furthermore, the pion and gluon corrections were also included to treat the baryons from strong interaction more realistically. The strengths of the confinement potentials for u, d, c quarks, were fixed by the masses and radii of baryons from the observations after considering three different constituent quark masses.

With respect to the nuclear many-body system, the baryons interact with each other in the hypernucleus via exchanging the scalar and vector mesons between the quarks in different baryons. The coupling constants between the vector mesons and u, d quarks have been obtained by fitting the ground-state properties of several double magic nuclei. The Λ_c^+N potential was very significant to study the properties of single-Λ_c^+ hypernuclei, which were decided by the coupling strength between the ω meson and the Λ_c^+ baryon. Therefore, two schemes were adopted in this work. The first one was that the naive quark counting rule was adopted, where $g_{\omega\Lambda_c^+} = 2/3 g_{\omega N}$. In the second one, the conclusion of the latest lattice simulations provided a good reference, which pointed out that the Λ_c^+N potential was just one-half of the ΛN potential in $^{209}_{\Lambda_c^+}$Pb with the single-folded potential method. Finally, two kinds of parameter sets were obtained, named as QMF-NK1C, QMF-NK2C, QMF-NK3C, and QMF-NK1C′, QMF-NK2C′, QMF-NK3C′, respectively, with different constituent quark masses.

The properties of single-Λ_c^+ hypernuclei were systematically calculated from the light to heavy mass region. The nuclear many-body systems became more bound when the Λ_c^+ baryons were included for QMF-NK1C, QMF-NK2C, and QMF-NK3C parameter sets. The rms radii of Λ_c^+ baryon density distribution were much smaller than those of protons and neutrons. It means that the Λ_c^+ baryon was inside of the Λ_c^+ hypernuclei. When the lattice simulation results were used, the Λ_c^+N potential did not bind so deeply. There was no bound state of heavy Λ_c^+ hypernuclei because of the strong repulsive contribution from Coulomb force up to $A \approx 50$. These results were consistent with the recent calculations by the RMF model, the HAL QCD group, and the perturbative many-body method.

The single-Λ_c^+ energies were also studied when the Λ_c^+ baryons were fixed at particular angular momenta. The Λ_c^+ baryon can occupy a very high angular momentum state when the coupling constants between the ω meson and the Λ_c^+ baryon were adopted by naive quark counting rules. Meanwhile, there were only $1s_{1/2}$ states with QMF-NK1C′, QMF-NK2C′, and QMF-NK3C′ sets, where shallow Λ_c^+N potentials were generated by scalar meson, vector mesons, and the Coulomb field from HAL QCD data.

The strength of the Λ_c^+N potential is the significant quantity in investigating the properties of single-Λ_c^+ hypernuclei, which cannot be determined by experimental observations very well now. In this work, two schemes were adopted, which have very large differences for heavy nuclei system. The relevant experiments about Λ_c^+ hypernuclei are expected to be done, especially in the heavy mass region to determine the magnitude of the Λ_c^+N potential.

ACKNOWLEDGMENTS

J.H. is very grateful to Ying Zhang for a careful reading of this manuscript. This work was supported in part by the National Natural Science Foundation of China (Grants No. 11775119 and No. 11675083) and the Natural Science Foundation of Tianjin.

[1] M. Danysz and J. Pniewski, Philos. Mag. **44**, 348 (1953).
[2] O. Hashimoto and H. Tamura, Prog. Part. Nucl. Phys. **57**, 564 (2006).
[3] A. Feliciello and T. Nagae, Rep. Prog. Phys. **78**, 096301 (2015).
[4] A. Gal, E. V. Hungerford, and D. J. Millener, Rev. Mod. Phys. **88**, 035004 (2016).
[5] R. Hayano, T. Ishikawa, M. Iwasaki, H. Outa, E. Takada, H. Tamura, A. Sakaguchi, M. Aoki, and T. Yamazaki, Phys. Lett. B **231**, 355 (1989).
[6] T. Nagae, T. Miyachi, T. Fukuda, H. Outa, T. Tamagawa, J. Nakano *et al.*, Phys. Rev. Lett. **80**, 1605 (1998).
[7] S. Aoki *et al.*, Prog. Theor. Phys. **89**, 493 (1993).
[8] P. Khaustov, D. E. Alburger, P. D. Barnes, B. Bassalleck, A. R. Berdoz, A. Biglan *et al.* (The AGS E885 Collaboration), Phys. Rev. C **61**, 054603 (2000).
[9] M. Yamaguchi, K. Tominaga, Y. Yamamoto, and T. Ueda, Prog. Theor. Phys. **105**, 627 (2001).
[10] K. Nakazawa *et al.*, Prog. Theor. Exp. Phys. **2015**, 033D02 (2015).
[11] T. Gogami *et al.*, Phys. Rev. C **93**, 034314 (2016).
[12] M. Danysz *et al.*, Phys. Rev. Lett. **11**, 29 (1963).
[13] D. J. Prowse, Phys. Rev. Lett. **17**, 782 (1966).
[14] S. Aoki *et al.*, Prog. Theor. Phys. **85**, 1287 (1991).
[15] J. K. Ahn *et al.*, Phys. Rev. C **88**, 014003 (2013).
[16] I. Vidaña, A. Polls, A. Ramos, M. Hjorth-Jensen, and V. G. J. Stoks, Phys. Rev. C **61**, 025802 (2000).
[17] I. Vidaña, A. Polls, A. Ramos, and H.-J. Schulze, Phys. Rev. C **64**, 044301 (2001).
[18] E. Hiyama and T. Yamada, Prog. Part. Nucl. Phys. **63**, 339 (2009).
[19] E. Hiyama, T. Motoba, T. A. Rijken, and Y. Yamamoto, Prog. Theor. Phys. Suppl. **185**, 1 (2010).
[20] E. Hiyama, Y. Yamamoto, T. Motoba, Th. A. Rijken, and M. Kamimura, Phys. Rev. C **78**, 054316 (2008).
[21] R. Wirth, D. Gazda, P. Navrátil, A. Calci, J. Langhammer, and R. Roth, Phys. Rev. Lett. **113**, 192502 (2014).
[22] I. Vidaña, A. Ramos, and A. Polls, Phys. Rev. C **70**, 024306 (2004).
[23] D. J. Millener, Nucl. Phys. A **804**, 84 (2008).
[24] A. Li, E. Hiyama, X.-R. Zhou, and H. Sagawa, Phys. Rev. C **87**, 014333 (2013).
[25] H.-J. Schulze and T. Rijken, Phys. Rev. C **88**, 024322 (2013) and references therein.
[26] J. W. Cui, X. R. Zhou, and H.-J. Schulze, Phys. Rev. C **91**, 054306 (2015).
[27] X. R. Zhou, E. Hiyama, and H. Sagawa, Phys. Rev. C **94**, 024331 (2016).
[28] Y. Sugahara and H. Toki, Prog. Theor. Phys. **92**, 803 (1994).
[29] J. Mares and B. K. Jennings, Phys. Rev. C **49**, 2472 (1994).
[30] H. Shen, F. Yang, and H. Toki, Prog. Theor. Phys. **115**, 325 (2006).
[31] R. L. Xu, C. Wu, and Z. Z. Ren, J. Phys. G: Nucl. Part. Phys. **39**, 085107 (2012).
[32] T. T. Sun, E. Hiyama, H. Sagawa, H.-J. Schulze, and J. Meng, Phys. Rev. C **94**, 064319 (2016).
[33] M. Fortin, S. S. Avancini, C. Providência, and I. Vidaña, Phys. Rev. C **95**, 065803 (2017).
[34] Z. X. Liu, C. J. Xia, W. L. Lu, Y. X. Li, J. N. Hu, and T. T. Sun, Phys. Rev. C **98**, 024316 (2018).
[35] K. Tsushima, K. Saito, and A. W. Thomas, Phys. Lett. B **411**, 9 (1997).
[36] K. Tsushima, K. Saito, J. Haidenbauer, and A. W. Thomas, Nucl. Phys. A **630**, 691 (1998).
[37] K. Saito, K. Tsushima, and A. W. Thomas, Prog. Part. Nucl. Phys. **58**, 1 (2007).
[38] H. Shen and H. Toki, Nucl. Phys. A **707**, 469 (2002).
[39] J. N. Hu, A. Li, H. Shen, and H. Toki, Prog. Theor. Exp. Phys. **2014**, 013D02 (2014).
[40] J. N. Hu, A. Li, H. Toki, and W. Zuo, Phys. Rev. C **89**, 025802 (2014).
[41] C. Patrignani *et al.* (Particle Data Group), Chin. Phys. C **40**, 100001 (2016).
[42] C. B. Dover and S. H. Kahana, Phys. Rev. Lett. **39**, 1506 (1977).
[43] G. Bhamathi, Phys. Rev. C **24**, 1816 (1981).
[44] H. Bando and M. Bando, Phys. Lett. B **109**, 164 (1982).
[45] B. F. Gibson, C. B. Dover, G. Bhamathi, and D. R. Lehman, Phys. Rev. C **27**, 2085 (1983).
[46] H. Garcilazo, A. Valcarce, and T. F. Caramés, Phys. Rev. C **92**, 024006 (2015).
[47] K. Tsushima and F. C. Khanna, Phys. Lett. B **552**, 138 (2003).
[48] K. Tsushima and F. C. Khanna, Phys. Rev. C **67**, 015211 (2003).
[49] K. Tsushima and F. C. Khanna, J. Phys. G **30**, 1765 (2004).
[50] K. Tsushima, Phys. Rev. D **99**, 014026 (2019).
[51] Y. H. Tan, X. H. Zhong, C. H. Cai, and P. Z. Ning, Phys. Rev. C **70**, 054306 (2004).
[52] Y. H. Tan and P. Z. Ning, Europhys. Lett. **67**, 355 (2004).
[53] Y. A. Batusov *et al.*, JINR Preprint E1-10069 (JINR, Dubna 1976).
[54] Y. A. Batusov *et al.*, JETP Lett. **33**, 56 (1981).
[55] V. V. Lyukov, Nuovo Cimento A **102**, 583 (1989).
[56] J. Riedl, A. Schafer, and M. Stratmann, Eur. Phys. J. C **52**, 987 (2007).
[57] R. Shyam and K. Tsushima, Phys. Lett. B **770**, 236 (2017).
[58] G. Krein, A. W. Thomas, and K. Tsushima, Prog. Part. Nucl. Phys. **100**, 161 (2018).
[59] Y. R. Liu and M. Oka, Phys. Rev. D **85**, 014015 (2012).
[60] S. Maeda, M. Oka, and Y. R. Liu, Phys. Rev. C **98**, 035203 (2018).
[61] T. Inoue, N. Ishii, S. Aoki, T. Doi, T. Hatsuda, Y. Ikeda, K. Murano, H. Nemura, and K. Sasaki, Phys. Rev. Lett. **106**, 162002 (2011).
[62] K. Sasaki *et al.* (HAL QCD Collaboration), Prog. Theor. Exp. Phys. **2015**, 113B01 (2015).
[63] T. Miyamoto *et al.* (HAL QCD Collaboration), PoS LATTICE **2015**, 090 (2016).
[64] T. Miyamoto *et al.* (HAL QCD Collaboration), PoS LATTICE **2016**, 117 (2017).

[65] T. Miyamoto *et al.*, Nucl. Phys. A **971**, 113 (2018).
[66] J. Haidenbauer and G. Krein, Eur. Phys. J. A **54**, 199 (2018).
[67] H. Garcilazo, A. Valcarce, and T. F. Caramés, Eur. Phys. J. C **79**, 598 (2019).
[68] I. Vidaña, A. Ramos, and C. E. Jiménez-Tejero, Phys. Rev. C **99**, 045208 (2019).
[69] N. Barik, R. N. Mishra, D. K. Mohanty, P. K. Panda, and T. Frederico, Phys. Rev. C **88**, 015206 (2013).
[70] R. N. Mishra, H. S. Sahoo, P. K. Panda, N. Barik, and T. Frederico, Phys. Rev. C **92**, 045203 (2015).
[71] R. N. Mishra, H. S. Sahoo, P. K. Panda, N. Barik, and T. Frederico, Phys. Rev. C **94**, 035805 (2016).
[72] X. Y. Xing, J. N. Hu, and H. Shen, Phys. Rev. C **94**, 044308 (2016).
[73] X. Y. Xing, J. N. Hu, and H. Shen, Phys. Rev. C **95**, 054310 (2017).
[74] J. N. Hu and H. Shen, Phys. Rev. C **96**, 054304 (2017).
[75] J. J. Aubert *et al.* (EMC Collaboration), Phys. Lett. B **123**, 275 (1983).